CFAR Detectors for DVB-T Passive Radar in non-homogeneous scenarios

N. del-Rey-Maestre, D. Mata-Moya, J. Rosado-Sanz, P. Gómez-del-Hoyo and M.P. Jarabo-Amores
Signal Theory and Communications Department.
Superior Polytechnic School. University of Alcalá.
Alcalá de Henares, Madrid 28805, Spain.
Email: {nerea.delrey, david.mata, javier.rosado, pedrojose.gomez, mpilar.jarabo}@uah.es

Abstract—CFAR (Constant False Alarm Rate) detectors were designed and evaluated in non-homogeneous DVB-T (Digital Video Broadcasting-Terrestrial) passive radar scenarios. The CA-CFAR (Cell-Averaged CFAR) is the most widespread incoherent CFAR technique. CA-CFAR detector is optimal under the assumption of homogeneous interference, but CA-CFAR performance is degraded when this assumption is not fulfilled. As an attempt to design CFAR algorithms in non-homogeneous environment, VI-CFAR (Variability Index-CFAR) was proposed. CA-CFAR and VI-CFAR detectors were designed and evaluated in a simulated and real passive radar scenarios. The real data were acquired by IDEPAR demonstrator, a DVB-T passive radar system. Results confirm the suitability of VI-CFAR based solutions in passive radar scenarios providing detection probabilities much higher than the detection capabilities associated with CA-CFAR.

Keywords—Constant False Alarm Rate Techniques, Passive Radar System, Radar signal processing

I. Introduction

In recent years, the availability of new technological solutions has increased the interest of Passive Radar (PR) systems as an alternative solution to anticipate and prevent the multiple threats that European society faces, such as crime, terrorism or management of natural disasters. A PR is a radar system whose main objective is to detect targets and to estimate parameters (such as position or velocity) using commercial broadcast, communications systems (digital television, FM radio, digital audio, mobile phone, etc), and radar or radio-navigation signals as illumination sources, rather than using a dedicated radar transmitter [1]. These radars are multi-static systems composed of a receiver element and one or more Illuminators of Opportunity (IoOs) available in the environment.

In PR systems, multi-channel reception schemes are imposed due to the bistatic geometry of the radar and the lack of control over the transmitter. Usually, two channel are used: reference channel (to acquire the transmitted signal by the IoO) and surveillance one (to capture the target echoes). This kind of radars is based on the correlation of the delay and Doppler-shifted copies of the received signals from the IoOs and the target echoes, generating the Cross Ambiguity Function (CAF) at the output of the processing stage. The CAF will be a key tool to estimate the bistatic range and Doppler shift of the target in the detection stage.

Although PR systems present many advantages over active ones (low development and maintenance cost, low probability of intercept, small size, low weight, and easily deployed), high complexity processing signal systems are required to detect targets and extract their information due to the use of uncontrolled transmitters, multi-static geometry and signals that are not designed for radar applications.

In PR scenarios, the radar detection problem to be solved can be formulated as a binary hypothesis test, where the detector has to decide between target absence (null hypothesis, H_0) and target presence (alternative hypothesis, H_1). The Neyman-Pearson (NP) detector is extensively applied in radar problems, which maximizes the Probability of Detection (P_D) maintaining the Probability of False Alarm (P_{FA}) lower than or equal to a given value [2].

A possible implementation of the NP detector consist in comparing the Likelihood Ratio (LR), $\Lambda(\widetilde{\mathbf{z}})$, to a detection threshold estimated according to P_{FA} requirements (η_{lr}) [3], as is expressed in (1). Where $\widetilde{\mathbf{z}}$ is the complex observation vector provided by the radar receiver, and $f(\widetilde{\mathbf{z}}|H_0)$ and $f(\widetilde{\mathbf{z}}|H_1)$ are the detection problem likelihood functions under both hypotheses.

$$\Lambda(\widetilde{\mathbf{z}}) = \frac{f(\widetilde{\mathbf{z}}|H_1)}{f(\widetilde{\mathbf{z}}|H_0)} \underset{H_0}{\overset{H_1}{\gtrless}} \eta_{lr}(P_{FA}) \tag{1}$$

This approach requires a complete knowledge of the likelihood functions, and significant detection losses appear when the actual target and/or interference models differ from those assumed in the LR detector design [4] [5].

In passive radars, the processing stage provides the CAF that allows the estimation of the range and Doppler of a target in the following detector stage. The input to the target detector is a set of M range-Doppler surfaces, one per each Pulse Repetition Interval (PRI). For detecting a low fluctuating target in AWGN (Additive White Gaussian Noise), the squared magnitude of the output of the CAF, sampled at the instant where the ratio between the instantaneous power of the output signal to the average power of the output noise is maximum, is a sufficient statistic (the Doppler shift of the input signal with respect to the matched filter impulse response was assumed equal to zero).

Actually, moving targets with unknown Doppler are assumed. The result of the cross-correlation between the reference channel and the surveillance channel signals, is the ambiguity function of the transmitted signal, scaled and shifted to be centered on the time delay and Doppler shift corresponding

to the bistatic range and radial velocity of the target. So, for each range-Doppler cell, a threshold can be calculated as a function of the thermal noise of the system. However, in the target echo, clutter and interference residuals are inevitably present along all the system. If the detection threshold is calculated assuming only the thermal noise contribution, the clutter and other interference residuals would give rise to an increase on the P_{FA} value.

In radar literature, conventional radar detection schemes based on Constant False Alarm Rate (CFAR) techniques are applied to maintain the desired P_{FA} at a constant level in spite of clutter parameters variations. This parametric solution works on a cell by cell basis, estimating statistics of the interference by processing a group of reference cells close to the CUT (Cell-Under-Test) and adjusting the detection threshold according to the background interference [6]. However, the CFAR detection capabilities decrease significantly when the clutter and/or target statistical parameters are different from that assumed.

In some scenarios, a non-homogeneous environment due to the presence of multiple interfering targets and/or clutter edges is presented. In this case, a CA-CFAR detector suffers high performance degradation and do not guarantee the required P_{FA}. If one or more targets seep in the reference cells, the P_D decreased due to an increment in the adaptive threshold. The clutter edge effects are quite similar than target interference, mainly when low power is placed in CUT. In addition, range-doppler maps associated with PR systems are characterized by the high power samples along range dimension for zero Doppler shift (due to the Direct Path Interference (DPI) generated by the IoO, the ground clutter and the strong radar echoes provided by the big buildings) that can mask targets with low Doppler values. Some solutions have been proposed in the literature as an attempt to design CFAR algorithms in non-homogeneous environment. Great-Of CFAR (GO-CFAR) offers better performance in the clutter edge case, but it degrades the PD in interference target scene. The Small-Of CFAR (SO-CFAR) [6] reduces the target masking problem selecting the smallest reference window, furthermore when targets are placed in both reference windows, it gets a reduction in terms of P_D. Thus, with small number of reference cells and homogeneous environment, its behavior is worse than CA-CFAR and GO-CFAR techniques.

Other approach known as Variability Index CFAR (VI-CFAR) is proposed in [7]. It is based on the CA-CFAR, GO-CFAR and SO-CFAR techniques, and it provides a better performance in both homogeneous and non-homogeneous situations of clutter. VI-CFAR selects the group of reference cells as leading half or lagging half of reference cells, or all the available reference cells. Using this previous classification, this CFAR technique provides lower CFAR losses in homogeneous environment and robustness in non-homogeneous scene.

In this paper, CA-CFAR and VI-CFAR based detectors were evaluated in a DVB-T PR urban scenario. Different windowing techniques are used for estimating the background statistics:

- One-dimensional (1D) window: the reference window extends along range or Doppler dimension.
- Two-dimensional (2D) window: independent detectors using 1D reference windows along range and Doppler dimensions were combined using the AND operator in order to declare a target if and only if both detectors have decided in favour of H_1.

The real radar data analyzed in this paper were acquired by a technological demonstrator developed under project IDEPAR (Improved Detection techniques for Passive Radars), funded by the Spanish Ministry of Economy and Competitiveness (TEC2012-38701) [8]. This system is a passive bistatic radar that uses Digital Video Broadcasting-Terrestrial (DVB-T) transmitters as IoOs. The radar scenario was located at the roof of the Polytechnic School (University of Alcalá), with the objective of detecting terrestrial vehicles. Results confirm that the VI-CFAR based detectors provides in passive radar scenarios a higher probability of detection, controlling CFAR losses and fulfilling the P_{FA} requirement, than the conventional CA-CFAR solution.

II. IDEPAR Demonstrator: DVB-T passive radar system

A. IDEPAR Demonstrator Description

The IDEPAR (Improved Detection techniques for Passive Radars) project is a technological demonstrator developed in the Superior Polytechnic School of the University of Alcal, funded by the Spanish Ministry of Economy and Competitiveness under project TEC2012-38701 [8]. The main objective of this project is to carry out an intensive research in order to improve the detection capabilities of passive radars, taking into consideration the detection of aerial and terrestrial targets.

This system is a PR that uses a DVB-T transmitter as IoO, in order to acquire real bistatic signals in the UHF (Ultra High Frequency) band in a terrestrial radar scenario. The demonstrator has been implemented using the basic architecture of a PR, where the following components have been considered:

- Commercial antennas: one for the reference channel and one for the surveillance one. These antennas have been selected to have good gains, high return losses and high front-to-back ratios for the frequency band under study.
- The receiving chain is composed of commercial daughter boards, Analog-to-Digital Conversion (ADC) systems,a synchronization unit, and the required drivers for storing the acquired digitized samples in RAM (Random-access memory) in real time.
- Signal processing stage: Different signal processing algorithms have been implemented, in order to perform the test and assessment of the hardware components. In this work, the output of the CAF stage is analyzed to define suitable statistical models for detector design.

The IDEPAR demonstrator has been designed to acquire three consecutive channels to improve the system resolution. The filtering, processing and detection stages have been implemented off-line. In [8], more information about the IDEPAR demonstrator such as reception and processing stages, or system coverage and resolutions is detailed.

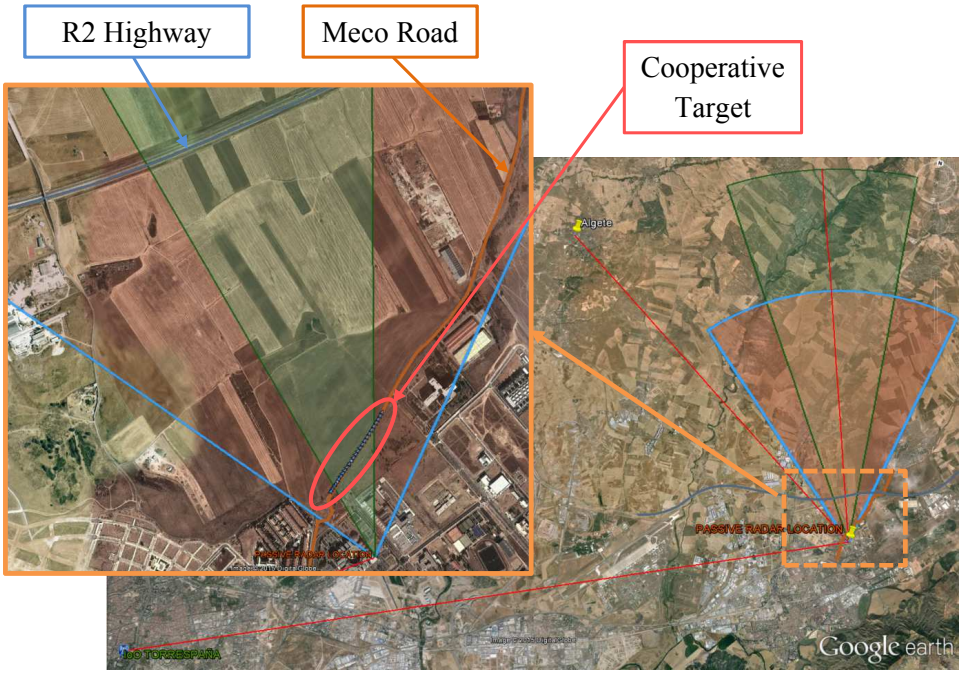

Fig. 1. Radar scenario. Green area: area of interest with a beamwidth equal to 30°. Orange area: area of interest with a beamwidth equal to 60°

B. Passive Radar scenario

The radar scenario was located at the roof of the Polytechnic school of the University of Alcalá, with the objective of detecting terrestrial vehicles. The Torrespaña transmitter was selected as IoO after a complete study of the available IoOs using WinProp software. In Figure 1 the Area of Interest (AoI) defined by the 3dB beamwidth of the receiver antenna (30°) is depicted together with the AoI associated with a beamwidth equal to 60°. The Meco road and the R2 highway are marked in brown and blue respectively. This scenario is characterized by the presence of big buildings with metal structure and a high traffic around them. In this paper, the data acquired on February 13, 2014 were used in the analysis.

In the experiment, a set of 30 seconds acquisitions were recorded. For each data acquisition, 120 range-Doppler matrices were generated using the following processing parameters:

- PRI: 250 ms.
- Integration time: 250 ms.
- CAF size: 401 Doppler shifts, $f_d \in [-799.744; 799.744]$ Hz and number of range bins equal to 1000 corresponding to a coverage distance of 9.45 km in the pointing direction.

In Figure 2, the normalized intensity (dB) of the output of the CAF stage for the PRI 1 is shown. As we can see, samples along range dimension for zero Doppler shift present high power values due to the Direct Path Interference (DPI) generated by the IoO, the ground clutter and the strong radar echoes provided by the big buildings. In this Doppler shift and the Doppler cells close to it, a non-homogeneous environment is considered. The range-Doppler matrix was split into different regions following a subjective criterion based on mean level estimation and the target position (Figure 2): Regions 1-A and 1-B correspond to high Doppler shift values

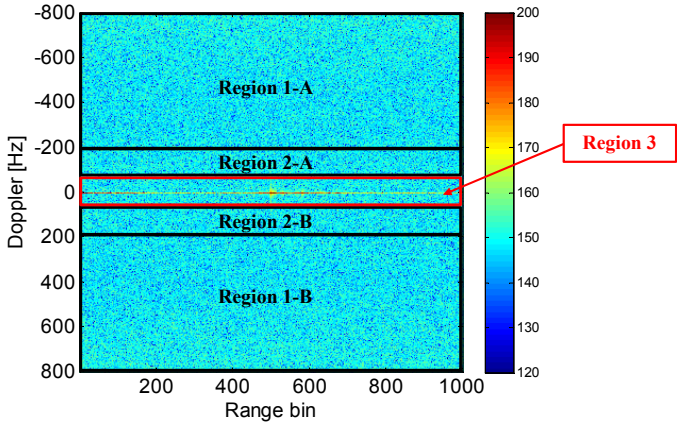

Fig. 2. Range-Doppler matrix of the recorded data

($f_d \in [-799; -200]$ Hz and $[200; 799]$ Hz respectively), Regions 2-A and 2-B are the target areas ($f_d \in [-200; -40]$ Hz and $[40; 200]$ Hz respectively) and Region 3 contains the zero Doppler shift ($f_d \in [-40; 40]$ Hz).

C. Case Study: Interference Statistical Analysis

For characterizing statistically the input of the radar detectors and the radar scenario detailed in the previous section, the Empirical Cumulative Distribution Function (ECDF) of the samples at the output of the PR processing stage (CAF matrix) was estimated and compared to those different theoretical distributions used in the radar literature to model the overall amplitude and/or intensity of the radar data [9]. Non-parametric tests such as the two-sample Kolmogorov-Smirnov (KS-test2) and the two-sample Cramér-von-Mises (CM-test2) criteria were applied to analyze the CDF applicability. Both methods are based on the estimation of the distance between

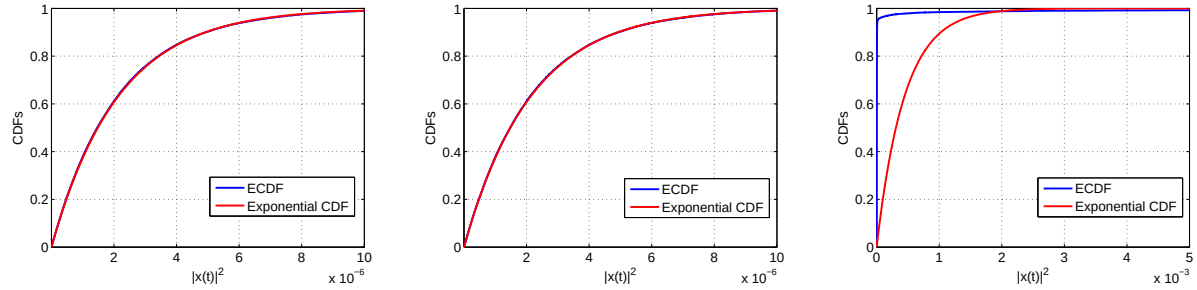

(a) Region 1-A. Intensity (b) Region 2-A. Intensity (c) Region 3. Intensity

Fig. 3. ECDF and Exponential CDF for the intensity of the recorded data

the empirical and theoretical CDFs, which will be compared to a threshold selected according to the significance level (the probability to reject H_0 when is true), α, and the samples sizes [9].

For saving space, only the results obtained for one PRI of only one acquisition was studied. The results can be extended to the rest of acquisitions. The range-Doppler matrix depicted in Figure 2 was analyzed, carrying out an independent statistical analysis for each region.

In Table I, the theoretical distributions that fulfill the considered goodness-of-fit test with a 5% of the significance level for the intensity of the recorded data are presented. Results show that Regions 1 and 2 follow a Exponential distribution, so a Gaussian clutter model is suitable. Because of that, a Gaussian model with zero mean and an associated clutter power $p_c = \sigma^2 \simeq 1.063 \cdot 10^{-6}$ for the in-phase and quadrature components was considered to design the detection stage.

Due to PR systems provide a zero Doppler, a non-homogeneous environment is considered in Region 3. This zero Doppler line has a mean power $p_c^{ZD} = 0.0046$ for the in-phase and quadrature components, almost 36 dB higher than the clutter power associated with Regios 1 and 2. These results can be checked in Figure 3, where the ECDF of the intensity and the Exponential CDF for Regions 1-A, 2-A and 3 are depicted.

In the considered radar scenario, terrestrial vehicles appear in the Regions 2-A and 2-B. The relationships between target and clutter power can be described as the Signal-to-Interference Ratio ($SIR = 10\log_{10}(p_s/(p_c + p_n)$, where p_n is the noise power obtained using the Clutter-to-Noise Ratio, $CNR = 10\log_{10}(p_c/(p_n))$.

TABLE I
THEORETICAL MODELS THAT FULFILL THE GOODNESS-OF-FIT TESTS FOR THE INTENSITY OF THE RECORDED DATA

Region	**Intensity**	
	Distribution	***Parameters***
Region 1-A	Exponential	$\lambda = 4.677 \cdot 10^5$
Region 2-A	Exponential	$\lambda = 4.683 \cdot 10^5$
Region 3	*	*
Region 2-B	Exponential	$\lambda = 4.702 \cdot 10^5$
Region 1-B	Exponential	$\lambda = 4.602 \cdot 10^5$

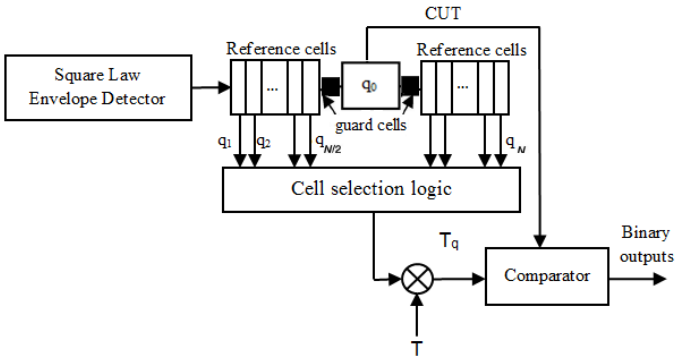

Fig. 4. CFAR detector general scheme

III. 1D CFAR TECHNIQUES IN HOMOGENEOUS AND NON-HOMOGENEOUS INTERFERENCE BACKGROUNDS

A. Cell Averaged CFAR (CA-CFAR)

The objective of CFAR detector is to maintain constant the false alarm probability even though noise and/or clutter variations exist in the receptor. This technique produces a threshold for each cell, adapting it against the noise and/or clutter around itself [10]. The threshold is set on a cell-by-cell basis, estimating interference statistics by processing a group of reference cells close to the CUT. Guard cells at both sides of the CUT are defined to avoid target echoes in the estimation of the clutter parameters. In Figure 4, the general operating scheme of CFAR detectors is presented, where:

- q_0 is the Cell Under Test (CUT).
- $[q_1, q_2, ..., q_N]$ are the reference cells.
- T is the multiplier factor fixed according to P_{FA} requirements.
- Cell selection logic is the rule defined by the type of CFAR detector.
- T_q is the adaptive threshold obtained by the product of T and the output of the cell selection logic.

Depends on how the adaptive threshold is computed, there are different CFAR detectors: Cell Averaging CFAR (CA-CFAR), Greatest Of CFAR (GO-CFAR), Smallest Of CFAR (SO-CFAR), Ordered Statistic CFAR (OS-CFAR) or Trimmed Mean (TM-CFAR) [6]. More recently, the Mean-to-Mean Ratio (MMR) test [11] and an Automatic Censored Cell

Averaging (ACCA) CFAR detector have been proposed. Some works dealing with fuzzy CFAR detector has been reported in the literature [12].

The CA-CFAR (Cell-Averaged CFAR) is the most widespread incoherent CFAR technique, whose thresholding constant can be calculated using 2. This detector is optimal under the assumption of independent and identically distributed samples with exponential probability density function [13]. These conditions are fulfilled when the interference is homogeneous white Gaussian noise (whose squared magnitude is exponentially distributed). In this case, the size of the reference window determines the noise power estimation error, and as this size increases, the detection probability approaches that of the optimum detector with a fixed detection threshold.

$$T = (P_{FA})^{\frac{-1}{N}} - 1 \tag{2}$$

As the size of the reference cells increases, the P_D approaches that of the optimum detector which is based on a fixed threshold. In homogeneous clutter, the CFAR detector requires a higher Signal to Interference Ratio (SIR) than the fixed threshold detector, due to the estimation of the clutter parameters using a set of N samples. This SIR increase is known as CFAR losses [13]. This parameter is very important for small values of N. On the other hand, big reference windows can increase the probability of enclosing target echoes, terrain returns (in coastal areas) or clutter returns from areas too far from the CUT. So a compromise solution must be determined, taking into consideration the characteristics of the radar scenario and the system resolution.

CA-CFAR performance degrades when the assumption of homogeneous reference window is violated. Different modifications have been proposed to overcome the problems associated with non-homogeneous noise backgrounds. They are intended for maintaining the desired P_{FA} when in the reference window the variance of the exponential noise samples changes (clutter edge) or there is any target. In all cases, the only interference present at the input of the envelope detector is assumed to be white Gaussian noise.

B. Variability Index CFAR (VI-CFAR)

Variability Index CFAR (VI-CFAR), proposed in [7], provides an adaptive threshold depending on the outcomes of the Variability Index (VI) and the Mean Ratio (MR) hypothesis tests achieving a good performance in both homogeneous and non-homogeneous situations of clutter.

In Figure 5, the VI-CFAR block diagram is depicted. The in-phase and quadrature (I and Q) signals are the entries of a square-law envelope detector. Like in the CA-CFAR technique, VI-CFAR method estimates the interference power in groups of cells surrounding the CUT and divides the group of reference cells as leading half (window A) or lagging half (window B) of reference cells. In this Figure, $N+1$ samples which correspond to N reference cells and a CUT (q_0) and the guard cells that are needed in order to prevent the reference cells corruption due to target power in the CUT are also presented. The adaptive threshold is computed as a constant multiply by the background noise/clutter power estimation. VI-CFAR

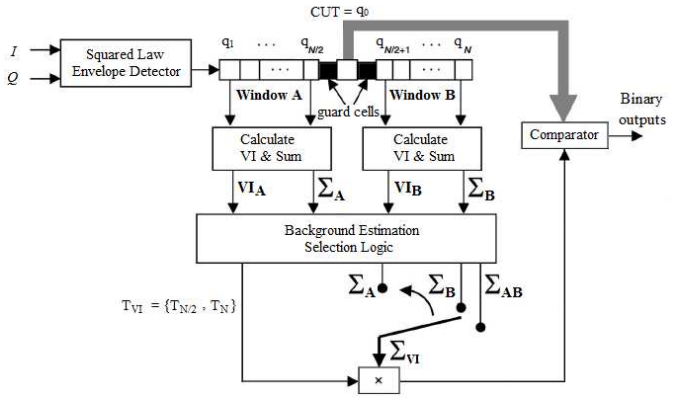

Fig. 5. VI-CFAR block diagram

detector estimates this power using a group of reference cells, in the same manner as CA-CFAR. The difference between them is that VI-CFAR split all available reference cells in two parts as commented, and decides between window A, B and all cells combination (window A-B). Shifting the content of the sample cells, VI-CFAR produces a decision for each CUT.

The statistic VI and the ratio MR are utilized by the VI-CFAR to determine the clutter homogeneity in the reference cells and select the best window or combination used for noise/clutter power estimation, respectively.

The VI threshold, considered as a second-order statistic, is computed for each window, leading (window A) and lagging (window B) using equation (3), where $\bar{X}$ is the arithmetic mean of the $n = N/2$ cells in each half-window.

$$VI^* = 1 + \frac{\hat{\sigma}^2}{\mu^2} = 1 + \frac{1}{n} \cdot \sum_{i=0}^{n} \frac{(X_i - \bar{X})^2}{\bar{X}^2} = n \cdot \frac{\sum_{n}^{i=1} X_i^2}{\left(\sum_{n}^{i=1} X_i\right)^2} \tag{3}$$

VI value is compared to K_{VI} threshold using the rule (4), deciding if CUT is placed in a homogeneous (non-variable) or non-homogeneous (variable) environment.

$$\begin{aligned} VI \leq MR \leq K_{VI} &\Rightarrow Nonvariable \\ VI > MR \leq K_{VI} &\Rightarrow Variable \end{aligned} \tag{4}$$

The MR is defined as the mean values ratio in both windows as shown in (5). Where $\sum_{i \in A} X_i$ and $\sum_{i \in B} X_i$ are the mean values for A and B window, respectively. These values increase when the presence of interfering target or clutter edge is placed in the A or B window, respectively.

$$MR = \frac{\bar{X}_A}{\bar{X}_B} = \frac{\sum_{i \in A} X_i}{\sum_{i \in B} X_i} \tag{5}$$

Decision rule expressed in (6) is used to decide if the means in both windows halves are the same or different.

TABLE II
SELECTION THE ADAPTIVE THRESHOLD FOR THE VI-CFAR DETECTOR

Decision	Window Variable	Different Means	VI-CFAR Adaptive Threshold
1	None	No	$C_N \cdot \sum_{AB}$
2	None	Yes	$C_{N/2} \cdot \max(\sum A, \sum_B)$
3	Leading	-	$C_{N/2} \cdot \sum_B$
4	Lagging	-	$C_{N/2} \cdot \sum_A$
5	Both	-	$C_{N/2} \cdot \min(\sum A, \sum_B)$

$$\begin{gathered} K_{MR}^{-1} \leq MR \leq K_{MR} \Rightarrow Same\ \ Means \\ MR < K_{MR}^{-1} \quad or \quad MR > K_{MR} \Rightarrow Different\ Means \end{gathered} \tag{6}$$

VI-CFAR detector uses the outcomes of both VI and MR hypothesis tests, for adapting the threshold as is shown in Table II. The multiplier constant is either T_N or $T_{N/2}$ where N corresponds to the number of reference cells in the complete window. If either leading or lagging half window is selected, the multiplier $T_{N/2}$ is used. These values are computed using equation (2) which is based on the number of reference cells and the desired P_{FA}.

The values K_{VI} and K_{MR} are chosen such that there is a high probability that the hypothesis test outcomes in a homogeneous environment will decide that each half window is non-variable and has the same mean as the other half reference window, respectively. These probabilities could be written by (7) and (8), where α_0 is defined as the error probability of classifying wrongly a homogeneous environment ranking as variable, and β_0 corresponds to the MR hypothesis test such that the means in both half windows are classified as different in a homogeneous environment. For reasonable performance in a non-homogeneous clutter, α_0 should be no larger than 5 to 10 times the desired P_{FA}. In practice, typical values of β_0 will not exceed 0.1 [7].

$$\alpha_0 = P[\, VI > K_{VI} |\, Homogenous\ \ Env.] \tag{7}$$

$$\beta_0 = 1 - P[\, \frac{1}{K_{MR}} \leq MR \leq K_{MR} |\, Homogenous\ \ Env.] \tag{8}$$

If the thresholds K_{VI} and K_{MR} increase, VI-CFAR gives a higher probability of making a correct decision when the environment is homogeneous but it decreases in terms of sensitivity for detecting non-homogeneous environments. The VI-CFAR detector presents also CFAR losses due to the use of a set of N samples to estimate the clutter background. The VI-CFAR technique provides slightly higher CFAR losses in homogeneous environments and robustness in non-homogeneous backgrounds.

TABLE III
ESTIMATED K_{VI} AND K_{MR} VALUES FOR A DESIRED $P_{FA} = 10^{-5}$ IN THE CASE STUDY ($p_c = 1.0630 \cdot 10^{-6}$, $\alpha_0 = 3.3 \cdot 10^{-5}$ AND $\beta_0 = 0.08$).

	$N = 8$	$N = 16$	$N = 32$	$N = 64$
K_{VI}	3.874	5.754	6.174	5.236
K_{MR}	3.746	2.472	1.876	1.556

C. Minimum required SIR in homogeneous and non-homgeneous scenarios

For evaluating the detection capabilities of the both detectors under study, detection curves (P_D vs SIR for a desired P_{FA}) were estimated assuming the following considerations:

- $N = \{8, 16, 32, 64\}$ reference cells were analyzed.
- $P_{FA} = 10^{-5}$ was selected.
- Montecarlo simulations were performed, guaranteeing an estimation error lower than 10% (10^5 samples were generated).
- According to the statistical analysis carried out in section II-C, Gaussian clutter samples with $p_c \simeq 1.063 \cdot 10^{-6}$ for the in-phase and quadrature components was considered. A Clutter to Noise Ration (CNR) equal to 20 dB is assumed to generate the interference signal without loss of generality.
- The extended Swerling II model was used to model the CUT as point target echoes acquired by passive radars [14]. SIRs ranging from 0 dB to 30 dB are studied.
- For the VI-CFAR detector, K_{VI} and K_{MR} parameters are estimated using Montecarlo simulations and the expressions (7) and (8), respectively. In Table III, the estimated values for the different number of reference cells are summarized, assuming $\alpha_0 = 3.3 \cdot 10^{-5}$ and $\beta_0 = 0.08$ (values recommended in [7]).

Two different data sets were generated in order to analyze the detection performance under homogeneous and non-homogeneous environments:

- Data set 1 - Homogeneous clutter: the pattern is a matrix ($65x10^5$) containing 64 reference cells generated assuming Gaussian clutter samples with p_c uniformly distributed and $CNR = 20$ dB, and a CUT generated under H_1 hypothesis with SIR belonging to $[0, 30]$ dB. In figure 6(a), the intensity of the data set 1 is presented.
- Data set 2 - Non-homogeneous clutter: as in the previous data set,the pattern is a matrix ($65x10^5$) containing 64 reference cells and the CUT generated assuming H_0 and H_1 hypothesis. In this case, the 43th cell were replaced by a Gaussian clutter with $p_c = 0.0046$ and $CNR = 20$ dB in order to generate a non-homogeneous environment similar to typical radar-doppler maps of PR systems. In figure 6(b), the intensity of the data set 2 is depicted.

In Figure 6, the red, purple, orange and blue rectangles corresponds to $N = 8, 16, 32, 64$ reference cells, respectively. In the non-homogeneous simulation (Figure 6(b)), reference cells equal to 32 and 64 includes the clutter samples with higher clutter power that can lead to an over-estimation of the adaptive threshold in the considered CFAR detectors.

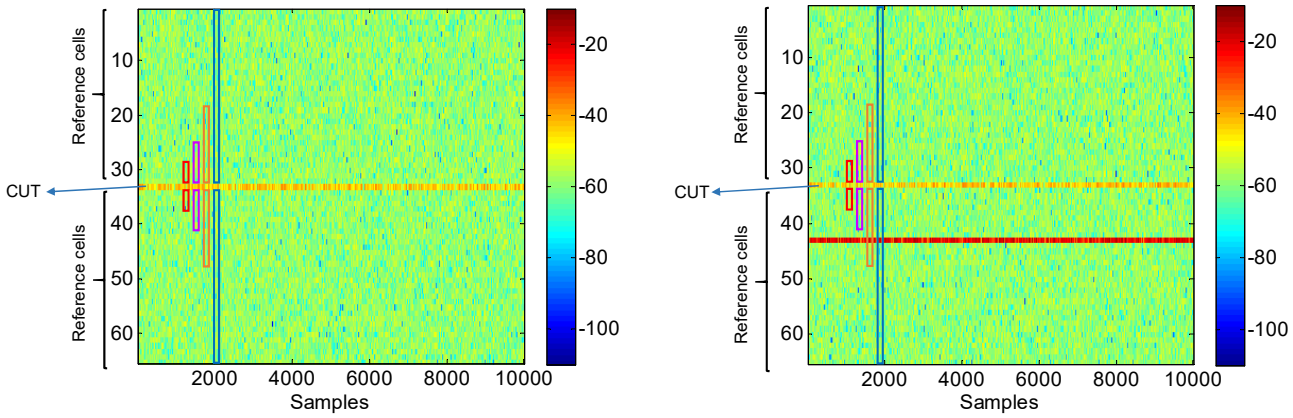

(a) Homogeneous clutter

(b) Non-homogeneous clutter

Fig. 6. Data sets generated to analyze the CFAR detection performance. Red: $N = 8$. Purple: $N = 16$. Orange: $N = 32$. Blue: $N = 64$

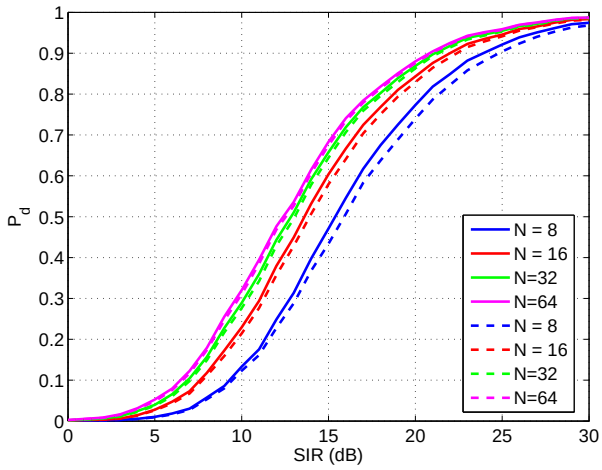

Fig. 7. Detection curves for $P_{FA} = 10^{-5}$ in homogeneous clutter. Solid line: CA-CFAR detector. Dash line: VI-CFAR detector

In Figures 7 and 8, the estimated detection curves for Data set-1 and Data set-2 are depicted, respectively. In a homogeneous environment, CA-CFAR and VI-CFAR detectors present similar detection performances. In both cases, as the number of reference cells increases, the CFAR losses decreases. VI-CFAR presents worse detection capabilities due to probability of making a decision distinct from 1 (Table II), where the number of reference cells used to estimate the adaptive threshold is reduced to $N/2$, so the CFAR losses are higher than the CA-CFAR basic detector. In the non-homogeneous environment, Figure 8(a) shows the $N = 8$ and $N = 16$ reference cells performance, where the reference window is composed of homogeneous interference samples (red and purple rectangles in Figure 6(b)). As we expect, CA-CFAR and VI-CFAR detectors provide same detection capabilities as in the homogeneous environment. However, in Figure 8(b), detection curves for $N = 32$ and $N = 64$ (orange and blue rectangles in Figure 6(b)) show the robustness of the VI-CFAR against non-homogeneous conditions, maintaining the detection capabilities.

TABLE IV
SIR REQUIRED FOR $P_D = 80\%$ AND $P_{FA} = 10^{-5}$ IN HOMOGENEOUS ENVIRONMENT

	$N = 8$	$N = 16$	$N = 32$	$N = 64$
CA-CFAR Detector	20.6 dB	18.7 dB	17.9 dB	17.4 dB
VI-CFAR Detector	21.3 dB	19.1 dB	18.1 dB	17.6 dB

TABLE V
SIR REQUIRED FOR A $P_D = 80\%$ AND $P_{FA} = 10^{-5}$ IN NON-HOMOGENEOUS ENVIRONMENT

	$N = 8$	$N = 16$	$N = 32$	$N = 64$
CA-CFAR Detector	20.6 dB	18.7 dB	$>$ 30 dB	$>$ 30 dB
VI-CFAR Detector	21.3 dB	19.1 dB	18.8 dB	17.9 dB

In Tables IV and V, the minimum SIRs required for $P_D = 80\%$ and $P_{FA} = 10^{-5}$ in homogeneous and non-homogeneous conditions are summarized. As we can see, CA-CFAR and VI-CFAR detectors provide similar detection capabilities when homogeneous interference is considered. However, for $N = 32$ and $N = 64$ in non-homogeneous environment, the CA-CFAR detector performance decreases significantly (for $N = 32$ and $SIR = 30$ dB, the P_D is equal to 33.55%. Under same conditions, for $N = 64$ and $SIR = 30$ dB, the P_D is equal to 53.60%).

As a compromise solution between CFAR loss and CUT-reference cells distance and taking into consideration the characteristics of the radar scenario and the system resolution, $N = 32$ is selected to estimate the clutter background and the adaptive threshold in the considered radar detectors.

IV. Experimental Results

A. CFAR Techniques in a simulated scenario

In this paper, different windowing techniques were considered for estimating the background statistics in the CFAR techniques:

- 1D Range CFAR detectors: the reference window extends along range dimension. The clutter power estimation can

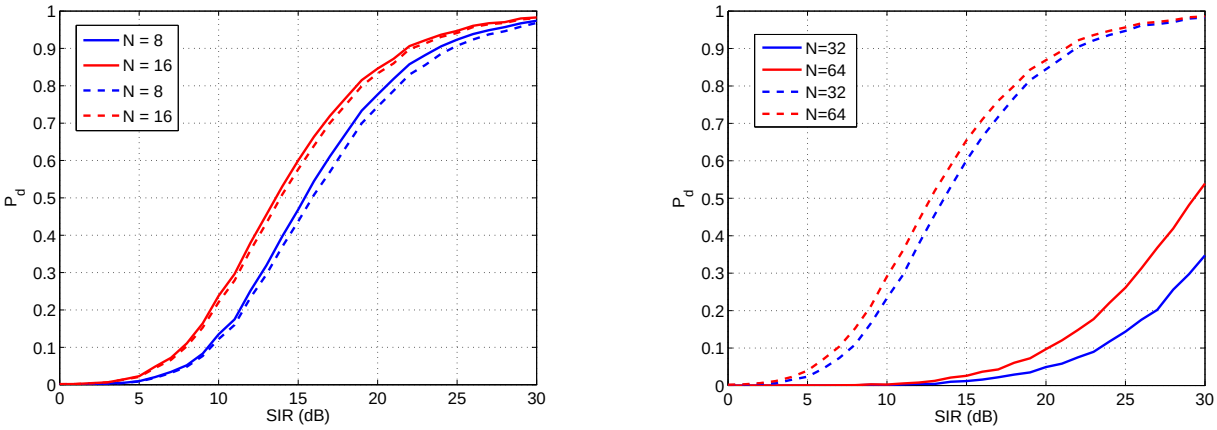

(a) Homogeneous reference cells

(b) Non-homogeneous reference cells

Fig. 8. Detection curves for $P_{FA} = 10^{-5}$ in non-homogeneous clutter. Solid line: CA-CFAR detector. Dash line: VI-CFAR detector

lead to false alarms due to strong returns, spread over Doppler dimension, associated with IoOs multipath.

- 1D Doppler CFAR detectors: the reference window extends along Doppler dimension. This solution can present false alarms associated with clutter echoes presented along range dimension for zero Doppler shift due to DPI and big metal buildings. In addition, these high returns can increase the estimated CFAR threshold and can mask targets with low Doppler values.
- 2D Range & Doppler CFAR: the combination of the outputs generated by both detectors has been considered to improve the detection performance. The AND logical operation has been applied in order to declare a target if and only if the target has been declared previously by both detectors.

Simulated scenario was considered to evaluate the 2D Range & Doppler CA-FAR and VI-CFAR using the characteristics of the radar scenario described in Section II-B and the clutter statistical parameters estimated in Section II-C maintaining a ratio of almost 36 dB between mean clutter power of Zero Doppler line and the Regions 1 and 2. Two Swerling II model targets with a SIR of 19 dB, associated to a P_D higher than 80% for $P_FA = 10^{-5}$ with 32 reference cells (Tables IV and V), were also simulated and represented in Figure 9. Target 1 is centered in 100th range cell with -40 Hz Doppler and Target 2 is centered in 200th range cell with -180 Hz Doppler. $N = 32$ reference cells were considered in both dimensions.

Figure 10 presents the detection results provided by 2D Range & Doppler CA-CFAR detector where the bottom figures correspond to zoomed areas of the Range-Doppler detection maps centered on the targets location. Although 1D Range CFAR scheme is able to detect both targets (Figure 10(d)), the target 1 is miss-detected by the 1D Doppler CFAR solution (Figure 10(e)) and consequently by the 2D Range & Doppler CFAR one (Figure 10(f)). This behavior is explained taking into consideration that target 1 is located in the blind area of the 1D Doppler CFAR associated to the considered reference cells ($N = 32$) and the estimated threshold when range cells

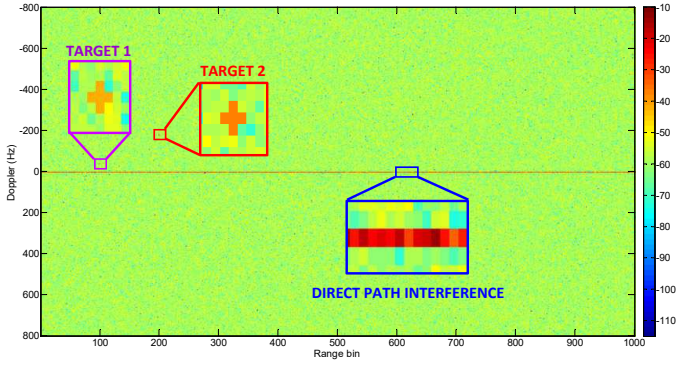

Fig. 9. Simulated Range-Doppler map with two Swerling II targets

of zero Doppler shift are included in the reference ones.

In Figure 11 the detection improvement associated with VI-CFAR based detectors is presented. As the VI-CFAR can adapt the threshold estimation in function of the homogeneity of the clutter in the reference cells, target 1 is also detected with the 1D Doppler CFAR scheme (Figures 11(b) and 11(e)). Then 2D Range & Doppler VI-CFAR detector (Figure 11(f)) clearly outperfoms 2D Range & Doppler VI-CFAR one (Figure 10(f)).

B. CFAR Techniques in DVB-T passive radar real data

In this Section CA-CFAR and VI-CFAR based detectors are evaluated using real data acquired by IDEPAR demonstrator described in Section II. Results are presented as the superimposition of the detector outputs in the 120 PRIs (acquisition time equal to 30 sec.). This superimposition allows the visual estimation of the targets trajectory, and displays all the false alarms detected through all PRIs.

To estimate P_{FA} and P_D, ground-truths at the output of the detector are required, but due to the complex nature of the electromagnetic back propagation process, targets dynamics and radar system, the real ground-truth is not available. Using the methodology described in [8], a ground-truth was generated for each CFAR detector using GPS data of cooperative

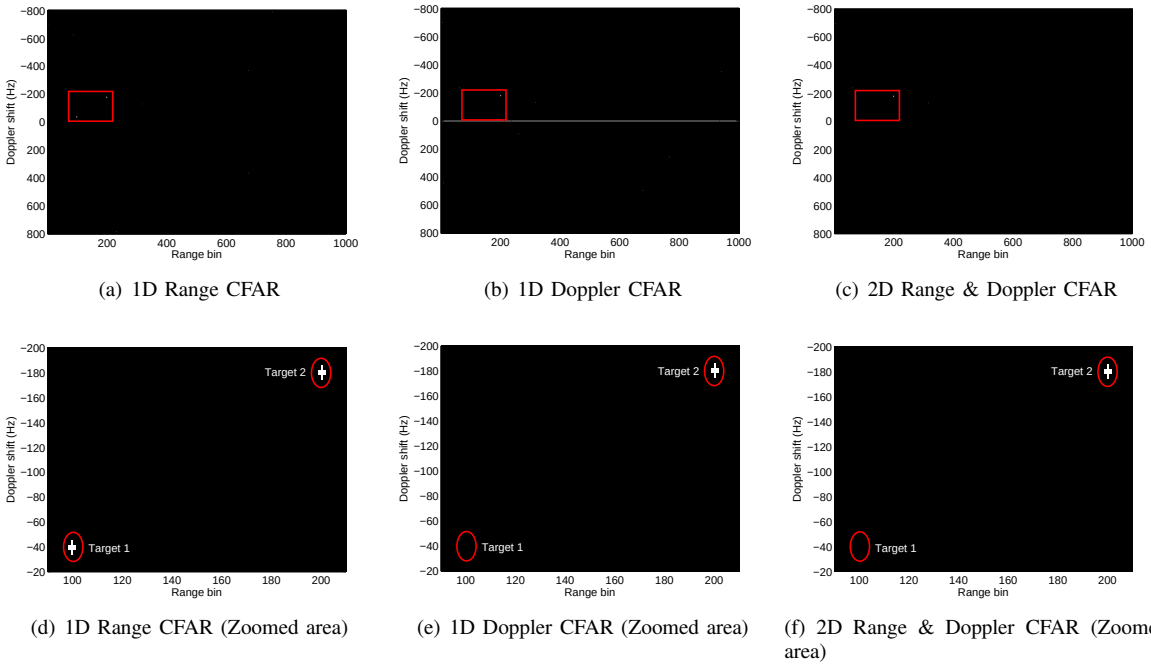

(a) 1D Range CFAR (b) 1D Doppler CFAR (c) 2D Range & Doppler CFAR

(d) 1D Range CFAR (Zoomed area) (e) 1D Doppler CFAR (Zoomed area) (f) 2D Range & Doppler CFAR (Zoomed area)

Fig. 10. Considered CA-CFAR techniques applied to the simulated scenario

vehicles and visual information about non-cooperative targets present in Meco road during the acquisitions. For estimating the P_{FA}, target and big buildings contributions in the range-Doppler map were removed. Montecarlo techniques were applied, guaranteeing an estimation error lower than 10%.

In [8] detection and tracking capabilities of the IDEPAR demonstrator were verified. The considered detection schemes were based on 1D Range, 1D Doppler and 2D Range & Doppler CA-CFAR techniques. In order to avoid the blind area associated with CA-CFAR based solutions the number of reference cells in the Doppler dimension were very small ($N = 8$) at expense of higher CFAR losses and decreasing the detection probability. Figure 12 confirms the CA-CFAR problem of detecting targets with low Doppler values.

2D Range & Doppler VI-CFAR is able to improve the detection capabilities in the whole Range-Doppler map using reference windows with size enough to control the CFAR losses. The main advantage is that this scheme allows the determination of non-homogeneous areas in both dimensions. In Figure 13 the homogeneity decisions for PRI 1 are depicted where the meaning of the decision values are described in Table II. Clutter in range dimension is homogeneous with variation of clutter power means at both sides of CUT. Decisions in Doppler dimension are clearly characterized by the Zero Doppler line, making the decision 4 when leading (down) reference window included the Zero Doppler line and estimating clutter power of lagging (up) reference window and making the decision 3 when lagging (up) homogeneous reference window included the Zero Doppler line and estimating clutter power of leading (down) homogeneous reference window.

2D Range & Doppler VI-CFAR detection performance is presented in Figure 14. Results show that the target trajectories are better defined even for low values of Doppler shift and the

TABLE VI
P_{FA} AND P_D OBTAINED BY LR AND MLP DETECTORS WITH REAL BISTATIC RADAR DATA.

	P_{FA}	P_D
CA-CFAR AND Detector	$8.652 \cdot 10^{-6}$	49.52%
VI-CFAR AND Detector	$8.573 \cdot 10^{-6}$	67.65%

big metal buildings are also detected. Table VI confirms the suitability of the proposed VI-CFAR based detector in DVB-T passive radar scenarios providing a P_D much higher than that associated with CA-CFAR based solutions, fulfilling the P_{FA} requirements.

V. CONCLUSION

CFAR detectors were designed and evaluated in non-homogeneous DVB-T passive radar scenarios. In PR, the processing stage provides the CAF that generates the range-Doppler maps or inputs to the detector. These maps are characterized by strong values in the range cells with zero Doppler shift. In addition, in a radar scenario can be present multiple interfering targets resulting non-homogeneous backgrounds.

Conventional radar detection schemes are based on CFAR techniques to maintain the desired P_{FA} at a constant level in spite of clutter parameters variations. The CA-CFAR is the most widespread incoherent CFAR technique. The detection performance depends on the number of reference and the estimation error of the clutter statistics. As the reference window size decrease, CFAR losses are increased or the required SIR to maintain a given P_D is increased. CA-CFAR detector is optimal under the assumption of homogeneous

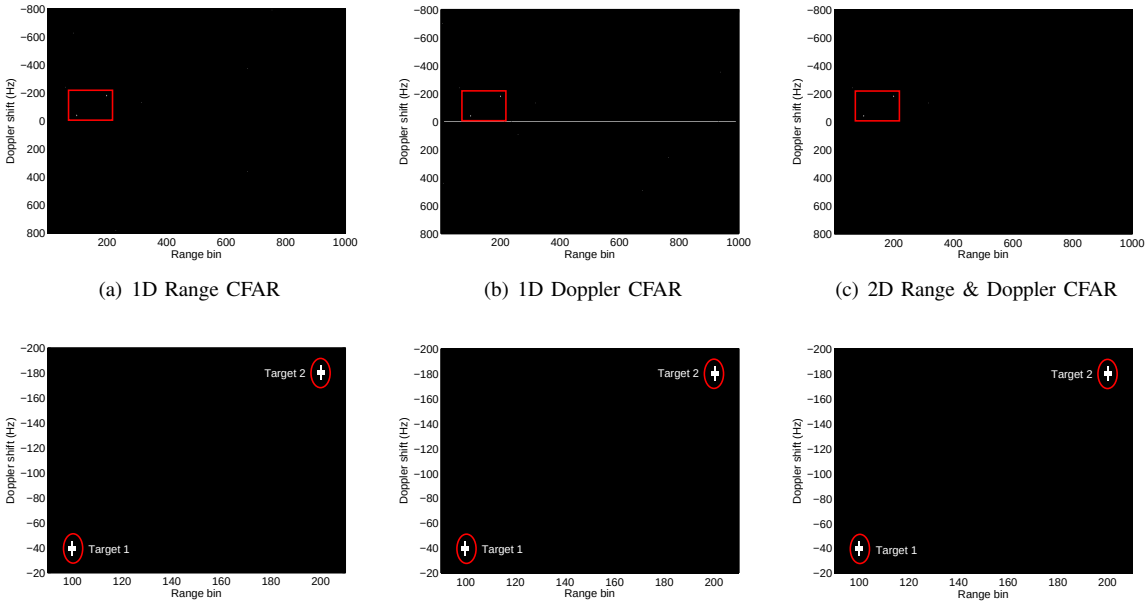

(a) 1D Range CFAR (b) 1D Doppler CFAR (c) 2D Range & Doppler CFAR

(d) 1D Range CFAR (Zoomed area) (e) 1D Doppler CFAR (Zoomed area) (f) 2D Range & Doppler CFAR (Zoomed area)

Fig. 11. Considered VI-CFAR techniques applied to the simulated scenario

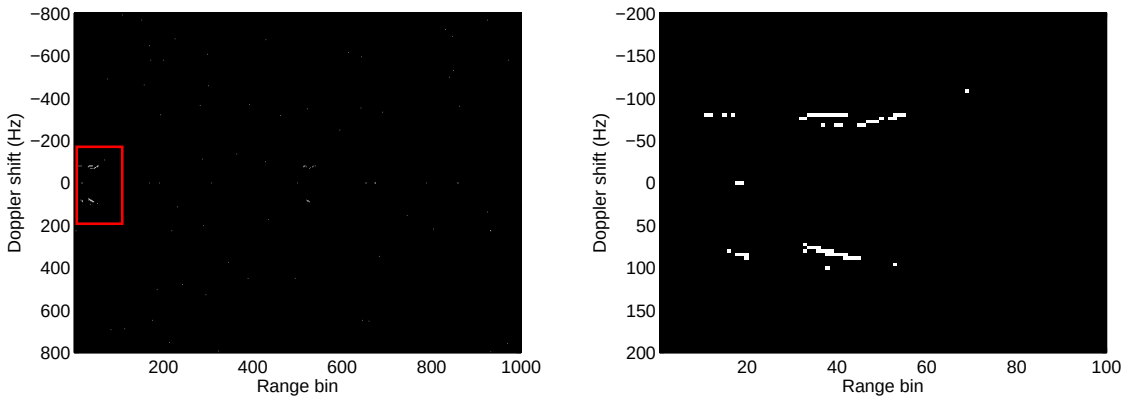

(a) Range-Doppler detection map (b) Zoomed area

Fig. 12. 2D Range & Doppler CA-CFAR detector applied to the real data acquired by IDEPAR demonstrator

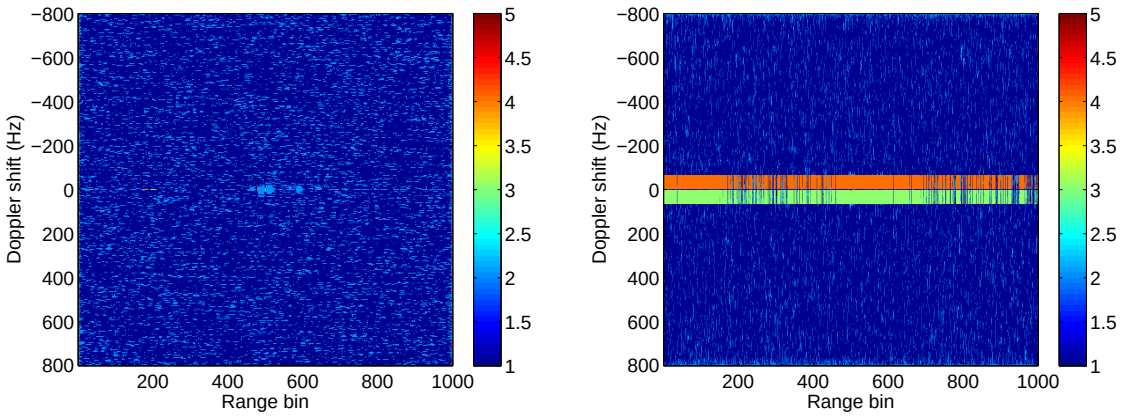

(a) Range dimension (b) Doppler dimension

Fig. 13. VI-CFAR homogeneity determination

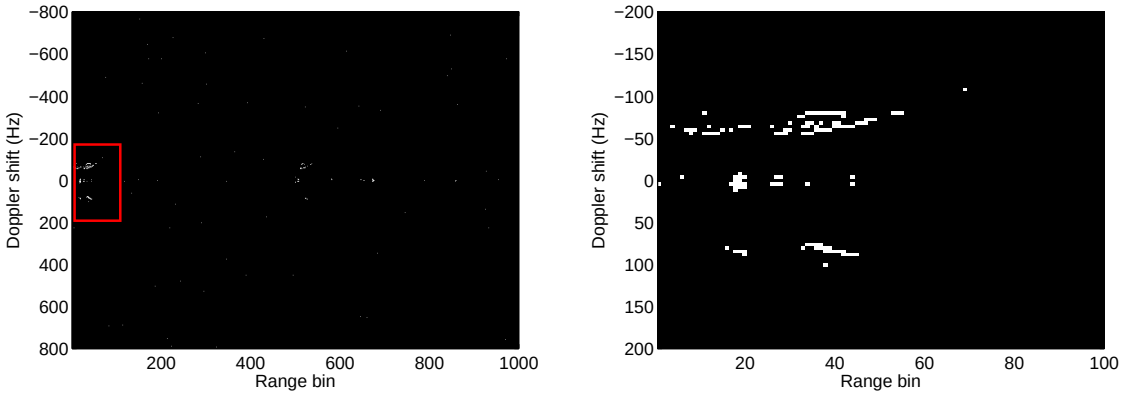

(a) Range-Doppler detection map (b) Zoomed area

Fig. 14. 2D Range & Doppler VI-CFAR detector applied to the real data acquired by IDEPAR demonstrator

interference, but CA-CFAR performance is degraded when this assumption is not fulfilled.

VI-CFAR was proposed to present robustness in homogeneous and non-homogeneous situations of clutter using the outcomes of the VI and the MR hypothesis tests. This combination provides slightly higher CFAR losses than CA-CFAR one for the same number of reference cells in homogeneous clutter however the detection performance is clearly outperformed in non-homogeneous scenarios.

Different CA-CFAR and VI-CFAR techniques were designed:

- 1D Range CFAR detectors: the reference window extends along range dimension.
- 1D Doppler CFAR detectors: the reference window extends along Doppler dimension.
- 2D Range & Doppler CFAR: independent detectors using 1D reference windows along range and Doppler dimensions were combined using the AND operator in order to declare a target if and only if both detectors have decided in favour of H_1.

The considered CFAR detectors were evaluated in a simulated and real passive radar scenarios. The case study corresponds to a measurement campaign carried out with the IDEPAR demonstrator, a DVB-T PR system. The radar scenario was located at the roof of the Polytechnic School (University of Alcalá), with the objective of detecting terrestrial vehicles. The simulated scenario was generated using the same clutter parameters as the real one with two Swerling targets with a SIR that guarantee a P_D higher than 80% for $P_{FA} = 10^{-5}$. Results for CA-CFAR based solutions reveal a blind area where targets with low values of Doppler shift are miss-detected associated with the presence of the high power values of range cells with zero Doppler shift in the reference windows extended along the Doppler dimension.

Results provided by 2D Range & Doppler VI-CFAR confirm the suitability of this detector in non-homgeneous backgrounds. The detection capability is very much better than the CA-CFAR detection performances. The main contribution of the considered 2D Range & Doppler VI-CFAR is the decision maps in function of VI and MR values that allows the capability of determining non-homogeneous areas in both dimensions and estimating the adaptive threshold to provide good detection probabilities controlling the CFAR losses.

ACKNOWLEDGMENT

This work has been supported by the Spanish "Ministerio de Economía y Competitividad", under project TEC2012-38701 and by the University of Alcalá, under project CCG2015/EXP070.

REFERENCES

[1] *IEEE Standard Radar Definitions*, IEEE aerospace and Electronics System Society Sponsored by the Radar System Panel, 2008.
[2] J. Neyman and E. Pearson, "On the problem of the most efficient test of statistical hypotheses," *Philosophical Transactions of the Royal Society of London*, vol. A 231, no. 9, pp. 289–337, 1933.
[3] H. V. Trees, *Detection, estimation, and modulation theory*, 2nd ed. Wiley, 2013, vol. Part I.
[4] V. Aloisio, A. di Vito, and G. Galati, "Optimum detection of moderately fluctuating radar targets," *IEEE Proceedings on Radar, Sonar and Navigation*, vol. 141, no. 3, pp. 164–170, 1994.
[5] A. di Vito and M. Naldi, "Robustness of the likelihood ratio detector for moderately fluctuating radar targets," in *IEE Proceedings on Radar, Sonar and Navigation*, vol. 146, no. 2, 1999, pp. 107–112.
[6] P. Gandhi and S. Kassam, "Analysis of CFAR processors in nonhomogeneous background," *IEEE Transactions on, Aerospace and Electronic Systems*, vol. 24, no. 4, pp. 427–445, 1988.
[7] M. Smith and P. Varshney, "Intelligent CFAR processor based on data variability," *IEEE Transactions on, Aerospace and Electronic Systems*, vol. 36, no. 3, pp. 837–847, 2000.
[8] M. Jarabo-Amores, J. Barcena-Humanes, P. G. del Hoyo, N. del Rey-Maestre, D. Juara-Casero, F. Gaitan-Cabaas, and D. Mata-Moya, "Idepar: a multichannel digital video broadcasting-terrestrial passive radar technological demonstrator in terrestrial radar scenarios," *IET Radar, Sonar and Navigation*, pp. 1–9, 2016.
[9] A. D. Maio *et al.*, "Measurement and comparative analysis of clutter for GSM and UMTS Passive Radar," *IET Radar, Sonar and Nav.*, vol. 4, no. 3, pp. 421–423, 2010.
[10] M. Skolnik, *Radar Handbook. Third Edition.* Mc-Graw Hill, 2008.
[11] T. Cao, "Design of low-loss CFAR detectors," in *Proceedings of IEEE Int Conference on Radar Systems*, vol. 1, 2008, pp. 712–717.
[12] H. El-Henawy, E. Abdoul-Fattah, M. Gamal, M. Attala, and A. Hafez, "A new fuzzy cfar processor for radar mtd systems," in *Proceedings of IEEE Aerospace Conference*, vol. 1, 2012, pp. 1–7.
[13] K. Ward, R. Tough, and S. Watts, *Sea Clutter: Scattering, the K Distribution and Radar Performance*. The Instituion of Engineering and Technology, 2006.
[14] K. Polonen and V. Koivunen, "Control symbol based fluctuating target detection in DVB-T2 Passive Radar Systems," *IEEE Radar Conference (RadarCon)*, pp. 1–5, 2013.